

# DARK CURRENT IMAGING EXPERIMENT IN AN L-BAND RF GUN

J.H. Shao<sup>1,2,\*</sup>, S. Antipov<sup>2,3</sup>, S.V. Baryshev<sup>2,3</sup>, H.B. Chen<sup>1</sup>, M.E. Conde<sup>2</sup>, D.S. Doran<sup>2</sup>, W. Gai<sup>2</sup>,  
 C. Jing<sup>2,3,#</sup>, W. Liu<sup>2</sup>, J.G. Power<sup>2</sup>, J.Q. Qiu<sup>2,3</sup>, J.R. Shi<sup>1</sup>, D. Wang<sup>1,2</sup>, F.Y. Wang<sup>4</sup>, C. Whiteford<sup>2</sup>,  
 E. Wisniewski<sup>2</sup>, and L.L. Xiao<sup>4</sup>

<sup>1</sup>Tsinghua University, Beijing 100084, China

<sup>2</sup>Argonne National Laboratory, Lemont, IL 60439, USA

<sup>3</sup>Euclid Techlabs LLC, Solon, OH 44139, USA

<sup>4</sup>SLAC National Accelerator Laboratory, Menlo Park, CA 94025, USA

## Abstract

The localized high electric field enhancement or low work function is the trigger for strong field emission, which however has yet been well experimentally studied. Using an L-band photocathode gun test stand at Argonne Wakefield Accelerator Facility (AWA), we've constructed an imaging beam line to observe field emission current from predefined emitters on cathode. Preliminary experiment results are present. Future plan is discussed.

## INTRODUCTION

Field emission (a.k.a. dark current) plays an important role in development of high gradient rf devices [1]. Elimination of sharp edges and achievement of smooth surface finishing in fabrication to alleviate the field emission is a standard practice to avoid rf breakdowns in operation of high gradient accelerating structures. Field emission has been well explained by the Fowler-Nordheim formula with quantum mechanism [1, 2], which is governed by three independent parameters, the local field enhancement factor  $\beta$ , the emitter area  $A_e$ , and the work function  $\phi$ .

Strong field emission observed in high gradient devices is dominated by emitters with high  $\beta$  or low  $\phi$  [1, 3]. Previous dc studies by field emission scanning microscopy (FESM) [4] and tunnelling atomic force microscopy (TUNA) [5] have revealed different types of emitters, such as particulates, surface protrusion, grooves with trapped contaminants, grain boundary, etc. However, to the best of the authors' knowledge, no systematic study to exactly locate emitters in rf devices has been carried out yet.

Locating field emitters in rf devices might help understand the fundamental mechanism of field emission. Moreover, if the rf breakdown spot can be identified simultaneously, it will also help reveal the relationship between field emission and breakdown.

## IMAGING PRINCIPLE

The gun used in this study is a 1.3 GHz L-band single cell photocathode gun with mountable cathode [6]. With 2 MW input power, the electric field on the flat cathode (noted as  $E_{\text{cathode}}$ ) can reach 70~100 MV/m depending on the cathode position.

A modified version of ASTRA code [7] is used to simulate the emission from the cathode as well as to track their movement to the downstream of the beam line. Due to the difficulties of accurately obtaining initial conditions, we've simulated the worst possible scenario (less constraint) of field emission on the cathode surface. In the simulation, we've assumed that 1) the initial kinetic energy of dark current is constant, 7 eV (Fermi energy of Cu), which is the maximum value of the real energy distribution [8]; 2) the emission angle follows uniform distribution over the entire 360° range; 3) the temporal structure of the emitted current is approximated by Gaussian distribution [9]; 4) space charge and mirror effect are not included; 5)  $E_{\text{cathode}}$  is 100 MV/m and  $\beta$  is 80; 6) the radius of emitter is 0.

Dark current can be emitted over 180° rf phase, resulting a wide energy spread and complicated beam dynamics. Although there is a sharp peak with the highest energy gain, the rms energy spread is ~300 keV as illustrated in Fig. 1. The trajectory of electrons emitted from the same position but different phases will be completely different, causing blurred images at downstream after acceleration by the gun, as shown in Fig. 2(a) and (b).

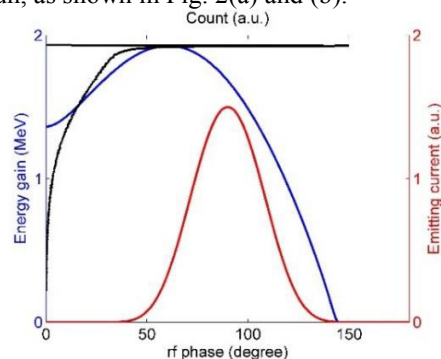


Figure 1: Energy gain (blue) and emitting current (red) at different rf phases and energy distribution (black).

To form a clear image, a straight-forward idea is to select electrons only from narrow phase band (or with narrow energy spread) and block others as shown in Fig. 2(c). This can be achieved by a solenoid (noted as the imaging solenoid) whose focusing depends on beam energy (thin lens approximation [10]):

$$\frac{1}{f} = \left( \frac{q}{2mc\beta\gamma} \right)^2 \int_l B^2 dz \quad (1)$$

where  $f$  is the focusing length;  $m$ ,  $q$ ,  $c\beta$ , and  $\gamma$  are mass, charge, speed and Lorentz factor of the particle;  $B$  and  $l$

\* jshao@anl.gov  
 # jingchg@anl.gov

are the field and effective length of the solenoid. When a collimator is applied at the focus, only electrons with corresponding energy will be selected, forming a clear image as shown in Fig.2 (d).

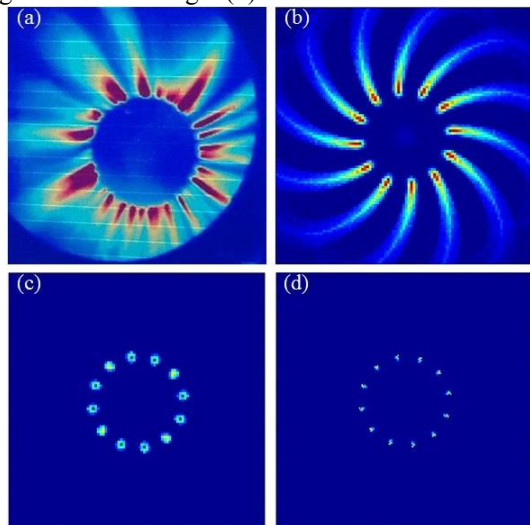


Figure 2: Dark current images. a) experimental result; b-d) simulation results of 12 emitters with 1 mm off-axis and separated by 30°. b) all; c) narrow energy spread; d) selected by the collimator.

Based on this principle, an imaging has been set up on an L-band photocathode gun test stand at AWA as shown in Fig. 3.

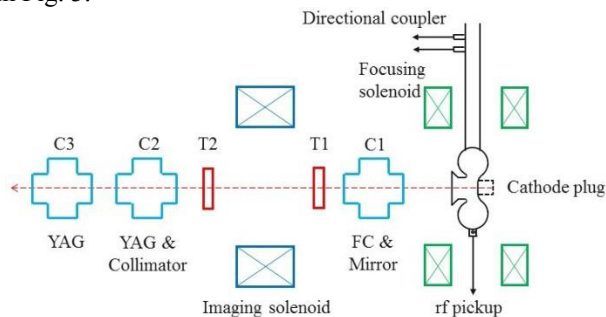


Figure 3: Layout of the L-band test stand.

## IMAGING PROPERTIES

### Magnification and Range

The dark current imaging system with a collimator acts as a pinhole camera. A real image can be captured at any position behind the collimator and the magnification increases with the distance between the YAG screen and the collimator. Due to space limitation of the beam line, the collimator and the imaging YAG screen have been set at 1.4 m and 1.9 m away from the cathode, respectively.

With a fixed distance, magnification is also adjustable through varying strength of the focusing solenoid of the gun (noted as the focusing solenoid). The imaging solenoid also needs to be adjusted accordingly to focus desired electrons at the collimator position. The maximum magnification is ~18 as illustrated in Fig. 4.

The imaging range is defined as the area on the cathode that can be imaged simultaneously. It's mainly limited by

the size of the beam pipe. Larger area can be partially imaged by bending the beam with a trim magnet between the collimator and the screen (does not exist now and will be added in forthcoming experiments).

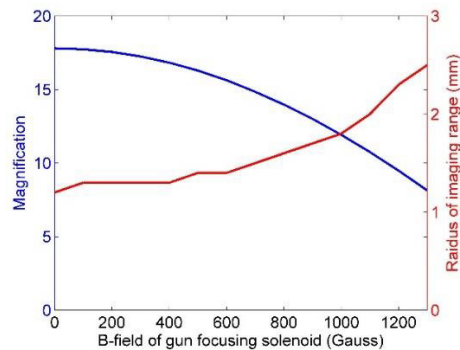


Figure 4: Magnification and imaging range of the system.

### Brightness

Brightness defined here is the percentage of emitted electrons that can pass through the collimator. In order to achieve the maximum brightness, the imaging solenoid strength should be adjusted to focus electrons with the highest energy at the collimator position according to energy distribution in Fig. 1. With fixed imaging solenoid strength, larger aperture of the collimator will lead to higher brightness and wider energy select range, as shown in Fig. 5.

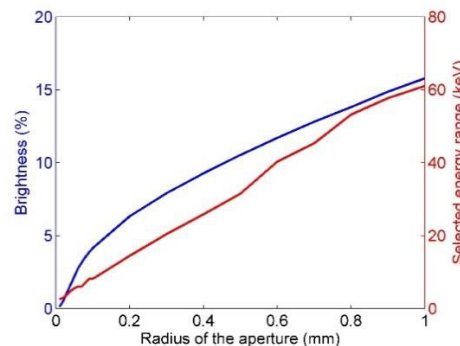


Figure 5: Brightness and selected energy range with different aperture radii (maximum on-axis B-field of the focusing solenoid is 1000 Gauss).

### Resolution

Resolution of an imaging system is the minimum distance between two emitters that can be distinguished. Because of the axial symmetry in this system, the trajectory of an electron strongly depends on its initial off-axis position. Thus in our study, the resolution can be further classified as the angular and radial resolutions which determine the minimum distinguishable distance between emitters at the same and different initial off-axis positions, respectively.

The angular resolution is defined as

$$R_{\theta} = 2 \times rms(\theta') \times r \quad (2)$$

where  $r$  is the off-axis position of an emitter on the cathode and  $\theta'$  is the rotation angle from the cathode to the screen of selected electrons.

Content from this work may be used under the terms of the CC BY 3.0 licence (© 2015). Any distribution of this work must maintain attribution to the author(s), title of the work, publisher, and DOI.

Due to spherical aberration of the imaging solenoid, the collimator will select electrons with lower energy originated from the inner emitters together with desired electrons with the highest energy from the outer emitters. The radial resolution is defined as

$$R_r = \min(r_{B,0} - r_{A,0}, r_B - r_A) \geq rms(r_A) + rms(r_B) \quad (3)$$

where  $r_0$  and  $r$  are off-axis positions on the cathode and the screen of two emitters A and B ( $r_{B,0} > r_{A,0}$ ).

Both resolutions can be improved by reducing the aperture radius as illustrated in Fig. 6. However, there is a low limit of the radial resolution. For example, for emitters at 1 mm off-axis position on the cathode, the best radial resolution is  $\sim 140 \mu\text{m}$ .

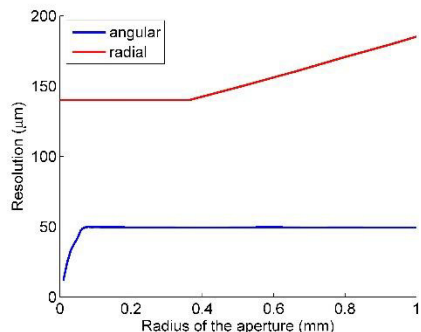


Figure 6: Resolution with different aperture radii of emitters with 1 mm initial off-axis (maximum on-axis B-field of the focusing solenoid is 1000 Gauss).

## PRELIMINARY EXPERIMENT

In the preliminary experiment, the tuner of the gun was not operational and the cathode position was fixed at  $\sim 3$  mm behind the gun surface for tuning, leading to  $\sim 3.2$  times lower electric field on the cathode than that on the cathode pipe edge as shown in Fig. 7. In order to enhance field emission from the cathode and calibrate the system, an arrow-like pattern was created on the cathode by sandblasting, as shown in Fig. 8(a). The roughness of the pattern was  $30\text{--}40 \mu\text{m}$ , much higher than that of other area on the cathode which was under  $1 \mu\text{m}$ . Dominated emission from this pattern was expected.

The aperture radius of the collimator was chosen to be 0.10 mm, 0.17 mm, and 0.25 mm. A PI-MAX intensified CCD [11] was applied to record images at C3.

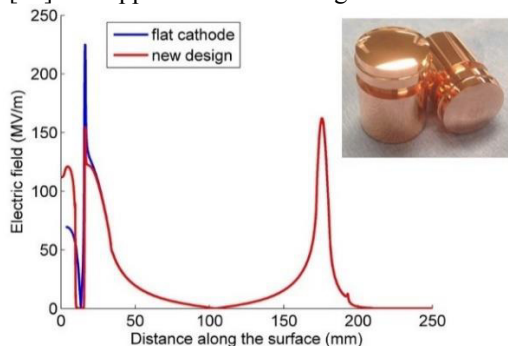


Figure 7: E-field along the surface with 2 MW input power. The peaks around 20 mm and 180 mm are caused by the cathode pipe edge and the gun iris, respectively; Inset: new designed cathodes.

In experiment, we didn't get expected image of the pattern because the roughness might be still not high enough to significantly enhance emission from the cathode. However, we got very clear images of emitters on the edge. Figure 8(b-d) clearly shows the resolution improvement by reducing the aperture radius. This demonstrates the imaging principle of the system.

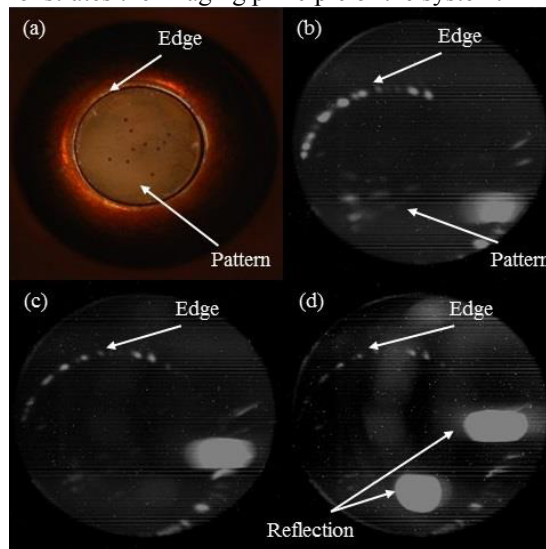


Figure 8: a) initial emitters on the cathode; b-d) dark current images with aperture radius of 0.25 mm, 0.17 mm, and 0.10 mm.

## FUTURE STUDY

Several improvements to this imaging system have been carried out. A new type cathode with small flat top and large rounding has been designed and fabricated at Tsinghua University, as shown in inset of Fig. 7. Together with the gun tuner, the field on the cathode can be remarkably enhanced. Besides, more trim magnets will be added to better control the beam. More experiments have been planned within a few months.

## CONCLUSION

A dark current imaging system has been built based on the energy/ emitting phase selection principle. The image properties have been studied. The preliminary experiment successfully demonstrates a clear dark current image. More experiments with improvement of the system are forthcoming.

## ACKNOWLEDGEMENT

We would like to thank Dr. Klaus Floettmann from DESY for his great help with the ASTRA code and useful discussion. The work is funded by the U.S. Department of Energy Early Career Research Program under project code LAB 11-572. Besides, the work by the AWA group is funded through the U.S. Department of Energy Office of Science under Contract No. DE-AC02-06CH11357. The work at Tsinghua University is supported by National Natural Science Foundation of China under Grant No. 11135004.

## REFERENCES

- [1] J. W. Wang and G. A. Loew, SLAC-PUB-7684 (1997).
- [2] R.H. Fowler and L.W. Nordheim, Proc. Roy. Soc. Lond. A119, 173 (1928).
- [3] H. Chen, et al., Phys. Rev. Lett. 109, 204802 (2012).
- [4] A. Dangwal, et al., J. Appl. Phys. 102, 044903 (2007).
- [5] V. Chatterjee, et al., Appl. Phys. Lett. 104, 171907 (2014).
- [6] C.H. Ho, et al., TUP33C, EPAC'98, Stockholm, Sweden (1998).
- [7] K. Floettmann, ASTRA-A space charge tracking algorithm; <http://www.desy.de/~mpyflo>
- [8] J.W. Gadzuk and E.W. Plummer, Rev. Mod. Phys. 45, 487-548 (1973).
- [9] R. Huang, et al., Phys. Rev. ST Accel. Beams 18, 013401 (2015).
- [10] M. Reiser, *Theory and Design of Charged Particle Beams*, (John Wiley & Sons, 2008), 89.
- [11] Princeton Instruments PI-MAX/ PI-MAX2 system; <http://www.princetoninstruments.com>